International Core Journal of Engineering Volume 12 Issue 3, 2026
ISSN: 2414-1895 DOI: 10.6919/ICJE.202603_12(3).0014

Study on Temperature Control Performance of Thermochromic Asphalt Pavement

Yan Sun[1,2,*]

[1] State Key Laboratory of Bridge Safety and Resilience, Beijing University of Technology, Beijing 100124, China

[2] The Key Laboratory of Urban Security and Disaster Engineering of Ministry of Education, Beijing University of Technology, Beijing 100124, China

[*]Corresponding Author

Abstract

Traditional asphalt pavements suffer from excessive heat absorption during summer months, which leads to structural damage and the Urban Heat Island effect. While conventional heat-reflective coatings can mitigate this issue, they often cause glare and result in overcooling during winter. This study develops a smart temperature-regulating asphalt pavement by integrating black thermochromic powder into a customized light-colored binder synthesized from petroleum resin and aromatic oil. The light-colored matrix is designed to overcome the masking effect of traditional black asphalt and enhance the inherent near-infrared reflectance of the material. Optical tests reveal that the thermochromic binder achieves a total solar reflectance of 15.46% at 40°C, representing a 4.38-fold increase compared to conventional 90# asphalt. Indoor solar simulation tests demonstrate that the thermochromic pavement reduces peak surface temperatures by 7.3°C in summer conditions. In winter simulations, the material slows the cooling rate by 34.2% and effectively delays the time to reach the freezing point by 47.7%. Furthermore, finite element method simulations across ten climatic regions in China confirm a cooling range between 4.4 and 7.3°C. The most significant effects are observed in high-radiation regions such as Lhasa with a 7.26°C reduction. The results indicate that the developed thermochromic asphalt provides an efficient and dual-season solution for pavement temperature regulation and urban heat mitigation.

Keywords

Thermochromic Asphalt; Solar Reflectance; Temperature Regulation; Numerical Simulation.

1. Introduction

Asphalt pavement is typically black. In hot summers, it absorbs a large amount of solar radiation. The absorption rate can exceed 95%[1]. Due to its high heat storage capacity, heat accumulates deep inside the pavement structure. This high-temperature environment damages the road structure and shortens its service life[2]. It also directly threatens driving safety. Currently, researchers have made progress in pavement temperature control. They use thermal properties to reflect heat, block heat, or store heat through phase-change materials. These methods help regulate surface temperatures and reduce the Urban Heat Island (UHI) effect[3–5].

Among various cooling methods, increasing solar reflectance is the most direct approach. It effectively reduces heat transfer into the pavement[6–8]. It also does not negatively affect the surrounding environment at night. However, current heat-reflective pavements face two main

ISSN: 2414-1895 DOI: 10.6919/ICJE.202603_12(3).0014

problems. First, high reflectance in visible light can cause glare issues[9]. Second, these pavements maintain high reflectance in winter. This makes the road surface too cold and affects safety[10]. A single coating cannot meet the different needs of summer and winter. Therefore, thermochromic materials have been introduced for smart temperature control.

Thermochromic materials change color reversibly based on temperature. Above a specific threshold temperature, they show high reflectance. Below that temperature, they show high absorbance[11–13]. Research shows that thermochromic asphalt can reduce pavement temperature by 6.6°C in summer[14]. In winter, it slows down the cooling process and prevents the road from reaching the freezing point. This reduces damage from extreme temperatures. It also lowers the impact of temperature fatigue. However, studies show a problem: the black base of traditional asphalt masks the optical properties of the thermochromic powder. As a result, the change in reflectance is not obvious[15]. Also, the high cost of the powder limits its use in large projects. Further research is needed to improve this technology.

To address the inherent limitations of conventional thermochromic asphalt, this study develops a novel thermochromic binder utilizing a synthetic light-colored matrix. This matrix, formulated from petroleum resin and aromatic oil, serves as a base for the integration of thermochromic functional powders. While maintaining mechanical performance comparable to traditional asphalt, the resulting material exhibits superior reflectance, emissivity, and heat capacity. Notably, the light-colored base significantly enhances the visual transition of the thermochromic additives, thereby optimizing dynamic thermal regulation.

The research further quantifies the influence of powder dosage on the binder's optical properties and validates its cooling performance through indoor solar radiation experiments. Finally, Finite Element Method (FEM) simulations under diverse meteorological conditions confirm the material's cooling efficiency across various climatic regions.

2. Materials and Test Methods

2.1 Materials

2.1.1 Thermochromic Materials

Thermochromic materials, synthesized from electron-transfer organic compounds, achieve reversible shifts in color and reflectance through temperature-induced molecular structural modifications[16]. This functionality is governed by a ternary system comprising a color former or electron donor that defines the base hue, a developer or electron acceptor that regulates color intensity, and a solvent-typically a phase-change material-used to calibrate the transition temperature. Generally, these materials are processed into powders with particle diameters ranging from 3μm to 10μm[17].

Among common variants such as red and blue, this study employs black thermochromic powder due to its widespread application and aesthetic compatibility with road infrastructure. The selected material features a transition threshold of 31°C. Below this limit, the powder retains a dark grey-black appearance; however, as temperatures surpass 31°C, it undergoes a gradual decolorization, ultimately transitioning to a grey-white state.

2.1.2 Thermochromic Asphalt Binder

In this study, a light-colored binder was developed as an alternative to conventional matrix asphalt and subsequently integrated with thermochromic powder to create a specialized modified asphalt binder with active temperature-regulating capabilities. This light-colored binder was synthesized through a polymer blending method, employing aromatic oil and petroleum resin as the primary matrix, with SBS modifier and a plasticizer added to enhance thermal stability[18,19].

The fabrication process involved preheating the petroleum resin at 175°C for 90 minutes and the aromatic oil at 160°C for 10 minutes, followed by blending the two components at 170°C for 10 minutes to reach a homogeneous state. Subsequently, preheated SBS particles were conditioned at 160°C for 20 minutes and introduced into the mixture via high-speed shearing at 1000 r/min for 10

ISSN: 2414-1895 DOI: 10.6919/ICJE.202603_12(3).0014

minutes at 170°C. The procedure concluded with the addition of a plasticizer and a final shearing stage at 4500 r/min at 175°C for 50 minutes. Based on preliminary research indicating that an excessive petroleum resin content of over 50% compromises binder performance, an optimized oil-to-resin ratio of 56:44 was established[20]. Combined with 10% SBS and 2% DBP plasticizer, the resulting binder conforms to the technical requirements for No. 90 base asphalt under JTG F40-2004.

To impart environmentally responsive properties, commercial black thermochromic powder was incorporated into the previously prepared light-colored binder. This additive facilitates the dynamic regulation of pavement temperature by modulating solar reflectance; specifically, the material lightens under high-temperature summer conditions to mitigate heat accumulation and darkens during winter to promote heat absorption and inhibit icing. To prepare the modified samples, the light-colored binder was liquefied at 135°C for 1 hour, after which thermochromic powder was added at mass fractions of 0%, 2%, 4%, 6%, and 8%. These mixtures were processed using a high-speed shear mixer at 140°C and 2000 r/min for 60 minutes to ensure uniform dispersion of the powder. For experimental identification, the samples are designated as Black-0, Black-2, Black-4, Black-6, and Black-8.

2.1.3 Thermochromic Asphalt Mixtures

To evaluate temperature-regulating performance at the mixture level, asphalt specimens were fabricated for indoor cooling tests, comprising both thermochromic asphalt and conventional asphalt mixtures. The thermochromic specimens featured a three-layer dense-graded structure consisting of an AC-13 surface layer with a nominal maximum aggregate size of 13.2 mm using Black-6 binder, followed by AC-16 middle and AC-20 bottom layers utilizing conventional 90# base asphalt. In contrast, the control specimens utilized 90# base asphalt across all three layers. The grading compositions for these layers are detailed in Table 1. All mixtures utilized basalt aggregates and mineral fillers adhering to relevant Chinese specifications.

Table 1. Aggregate gradation of AC-13 asphalt mixture used for the surface layer

Sieve size (mm)	Specification range (%)	Passing (%)
26.5	100–100	100.0
22.4	100–100	100.0
19.0	100–100	100.0
16.0	100–100	99.4
13.2	90–100	92.9
9.5	68–85	79.7
4.75	38–68	52.4
2.36	24–50	30.5
1.18	15–38	20.9
0.60	10–28	15.0
0.30	7–20	10.5
0.15	5–15	8.0
0.075	4–8	6.2

The Marshall design method was employed to establish a fixed optimal asphalt-aggregate ratio of 4.8%, with target air voids maintained at 4.0 ± 0.5% to ensure consistent volumetric properties. Specimens were constructed layer by layer via Marshall compaction, with each layer compacted to its design thickness. Emulsified asphalt served as the interlaminar bonding agent to integrate the

ISSN: 2414-1895 DOI: 10.6919/ICJE.202603_12(3).0014

layers into a unified cylindrical unit, consisting of a 4 cm surface, 5 cm middle, and 6 cm bottom layer. Following fabrication, the specimens were cured at room temperature prior to the cooling tests.

Fig. 1 Asphalt mixture samples

2.2 Test Equipment and Methods

2.2.1 Optical Tests

Spectral reflectance was measured across a scanning range of 300 nm to 2500 nm using a UV-Vis-NIR spectrophotometer with a diffuse reflection integrating sphere. For the test, the thermochromic binder was encapsulated between two 1 mm thick glass slides. Reflectance spectra were recorded first at room temperature and subsequently at 40°C, with the latter maintained by a temperature control device to ensure the sample remained above its switching threshold. Following ASTM E903-96, the weighted average method was applied to calculate the solar reflectance across the total spectrum (Rtotal, 300–2500 nm), ultraviolet range (Ruv, 300–400 nm), visible range (Rvis, 400–700 nm), and near-infrared range (Rnir, 700–2500 nm). The specific calculation formulas are defined as follows:

$$\mathrm{R}(\%) = \frac{\left(\sum_{i=1}^{n} \mathrm{R}(\lambda_i) E_{\lambda_i}\right) \lambda_i}{\sum_{i=1}^{n} E_{\lambda_i} \Delta\lambda_i} \tag{1}$$

where Eλ and Δλ denote the standard spectral irradiance distribution and the weighting function, respectively, as specified in ASTM E490.

2.2.2 Indoor Temperature-Controlled Solar-Simulation Test

To characterize temperature evolution at varying depths, measurement points were established on the specimen surface and at depths of 2 cm, 6 cm, and 12 cm. Temperature sensors were installed in pre-drilled holes, with the remaining voids filled with insulation cotton to minimize air convection. Prior to testing, the bottom and lateral surfaces of the specimen were encased in a glass wool layer at least 3 cm thick to suppress multi-directional heat loss. This insulation ensures predominant vertical heat flow, thereby highlighting the vertical heat transfer characteristics of the pavement structure. To eliminate interference from uncontrollable outdoor variables such as wind speed, air temperature fluctuations, and cloud cover, this study employed indoor simulation tests to evaluate cooling performance under a controlled single-variable environment. An artificial light system was constructed to replicate the heating effect of solar radiation on the pavement structure. By comparing thermochromic and conventional asphalt mixtures under identical radiation intensities, the analysis focused on variations in heating rates, peak temperatures, and internal temperature gradients. The experimental setup comprised an environmental chamber, an adjustable lamp stand, a 500 W iodine-

ISSN: 2414-1895 DOI: 10.6919/ICJE.202603_12(3).0014

tungsten lamp, K-type thermocouples, and a multi-channel data logger. With an emission spectrum spanning 150–4000 nm, the iodine-tungsten lamp effectively simulates the primary wavebands of solar radiation[21].

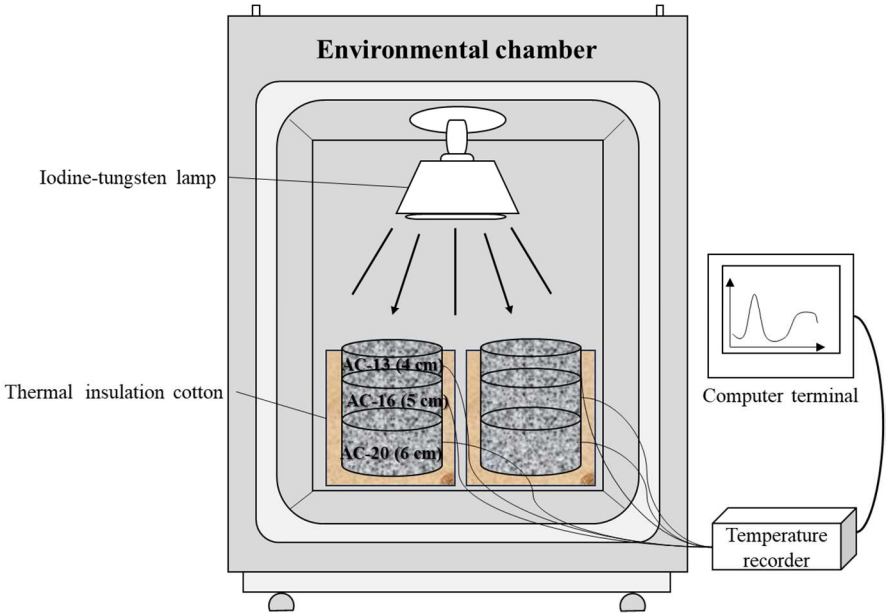

Fig. 2 Solar radiation simulation test setup

A 500 W iodine-tungsten lamp was selected as the radiation source due to its spectral characteristics, which closely simulate natural sunlight. Following the calculations from Eq. (2) and Eq. (3) based on typical clear summer days in Beijing, the equivalent irradiance was set at 653.76 W/m² for a 500-minute irradiation period. To ensure uniform surface heating, the lamp height was fixed at 40 cm and calibrated using a five-point method with a solar radiometer. Throughout the test, the environmental chamber was maintained at a constant temperature of 25°C.

$$QS(T) = \begin{cases} 1000\cos(\pi \dfrac{T-12}{14}) & 5 \le T \le 19 \\ 0 & \text{otherwise} \end{cases} \quad (2)$$

where QS is the solar radiation intensity (W/m²), and T is time (h).

$$E_L = \int Q_S dT = Q_L t_L \quad (3)$$

where EL is the radiant energy per unit area (W·h/m²), $Q_L$is the equivalent lamp irradiance (W/m²), and TL is the exposure time (h).

To simulate winter environments and evaluate the thermal preservation properties of thermochromic materials, test parameters were adjusted based on data from the National Meteorological Information Center (2022). First, the environmental chamber temperature was set to 20°C. Specimens were conditioned for 1 hour until their pavement surface temperatures stabilized, at which point the thermochromic materials had completely transitioned into a dark, heat-absorbing state. Next, the height of the lamps was increased to 65–70 cm to maintain the effective surface irradiance at 200

ISSN: 2414-1895 DOI: 10.6919/ICJE.202603_12(3).0014

W/m² ± 10 W/m², simulating a winter climate characterized by low temperatures and weak radiation. Under a constant ambient temperature of -20°C, the specimens were irradiated until their temperatures reached a steady state. The temperature recovery process was monitored in real-time using thermocouples embedded at various depths.

By comparing the heating curves of thermochromic samples with those of ordinary samples, their thermal insulation performance was analyzed. This process verified the material's heat retention effect during winter and its capability to mitigate the "winter overcooling" issue common in traditional reflective pavements.

2.3 Numerical Simulation for Outdoor Solar Radiation Test

2.3.1 Heat Transfer Theory of Asphalt Pavement

Heat transfer mainly consists of three basic forms: heat conduction, heat convection, and heat radiation. Asphalt pavement is a semi-exposed, multi-layer composite structure. Its temperature field is affected by solar radiation, air temperature, wind speed, and the thermal properties of the materials[22]. From the perspective of heat exchange mechanisms, the energy balance of the pavement can be divided into two processes. The first is the exchange of radiation and convection between the road surface and the external environment. The second is the process of heat conduction within the pavement structure. Heat exchange between the road surface and the outside involves several types of radiation. These include solar short-wave radiation (both direct and scattered), atmospheric backward radiation, and long-wave radiation emitted by the pavement. It also includes convective heat transfer caused by air flow. Among these, solar short-wave radiation is the primary heat source that causes the pavement temperature to rise. Inside the pavement, heat is transferred downward layer by layer through conduction. This creates a temperature gradient along the depth of the road.

$$q_{net} = q_s + q_a - q_r - q_c \tag{4}$$

Where qnet is the net heat flux absorbed by the pavement in W/m²; qs is the absorbed solar short-wave radiation in W/m²; qa is the absorbed atmospheric backward radiation in W/m²; qr is the long-wave radiation emitted outward by the pavement in W/m²; and qc is the convective heat transfer between the pavement and the air in W/m².

Solar radiation is the primary energy source for pavement heating, and the ability of the pavement to absorb solar energy depends mainly on the absorption rate of its surface.

$$q_s = \alpha \cdot G = (1 - \gamma) \cdot G \tag{5}$$

Where α is the solar energy absorption rate; γ is the solar reflectance of the pavement surface; and G is the total solar radiation intensity in W/m².

The pavement transfers heat through contact with the air due to temperature differences. This process is strongly affected by wind speed and generally follows Newton's Law of Cooling:

$$q_c = h_c(T_s - T_a) \tag{6}$$

Where hc is the surface convective heat transfer coefficient; Ts is the pavement surface temperature; and Ta is the ambient air temperature.

ISSN: 2414-1895 DOI: 10.6919/ICJE.202603_12(3).0014

In practical applications, hc is often expressed as:

$$h_c = 3.8v + 5.8 \tag{7}$$

Where v is the wind speed.

The pavement, as a thermal body, emits long-wave radiation to the atmosphere and simultaneously receives radiation from the atmosphere. The net result is usually expressed as:

$$q_{rad} = q_a - q_r = \epsilon\sigma\left(T_s^4 - T_{sky}^4\right) \tag{8}$$

Where ε is the pavement emissivity; σ is the Stefan-Boltzmann constant, which is equal to 5.67 x 10-8 W/(m²·K⁴), and T_{sky} is the effective sky temperature.

When the road surface gains energy and creates a temperature difference, heat spreads to the interior through thermal conduction. The asphalt pavement is considered an isotropic, homogeneous, and continuous medium. Its internal temperature field follows Fourier's Law. According to transient heat conduction theory, the governing equation for the three-dimensional temperature field is:

$$\rho C_p \frac{\partial T}{\partial t} = \frac{\partial}{\partial x}\left(k_x \frac{\partial T}{\partial x}\right) + \frac{\partial}{\partial y}\left(k_y \frac{\partial T}{\partial y}\right) + \frac{\partial}{\partial z}\left(k_z \frac{\partial T}{\partial z}\right) \tag{9}$$

In practical pavement engineering, since the horizontal (x, y) dimensions of the road are much larger than its vertical depth (z), the process is usually simplified into a one-dimensional heat transfer problem:

$$\rho C_p \frac{\partial T}{\partial t} = k\frac{\partial^2 T}{\partial z^2} \tag{10}$$

Where ρ is the material density; Cp is the specific heat capacity; and k is the thermal conductivity.

2.3.2 Geometric Model and Boundary Conditions in Finite Element Simulation

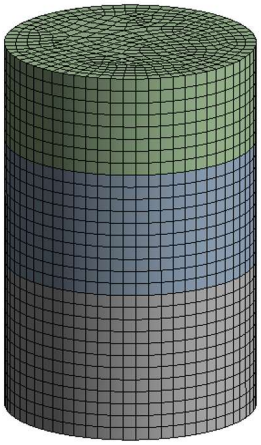

Fig. 3 The geometric model in numerical simulation

ISSN: 2414-1895 DOI: 10.6919/ICJE.202603_12(3).0014

This study uses the finite element analysis software ANSYS to construct a 3D transient heat conduction model to simulate the temperature field evolution of thermochromic asphalt pavement under outdoor solar radiation conditions. The geometric model in the simulation was based on the actual dimensions of the samples used in outdoor solar radiation experiments, as shown in Fig. 3. To accurately capture the temperature gradient along the thickness of the pavement, the model was divided into layers along the depth direction. Thermal solid elements were used for meshing, with refined mesh around the surface layers.

This study involves two types of materials: thermochromic asphalt mixture and regular asphalt mixture. The thermal conductivity and specific heat capacity of these materials were tested using the Hot Disk thermal conductivity meter. The thermal properties of each layer material are listed in Table 2.

Table 2. Thermophysical parameters of each asphalt surface layer

Thermophysical parameters	Thermochromic Asphalt Top Layer	Base asphalt surface layer	Asphalt middle and lower layers
Density (kg/m^{-3})	2300	2400	2400
thermal conductivity (W/(m·K))	1.1415	1.2	1.8
Specific heat capacity (J/kg·K)	985.5	920	1000
Reflectivity (<31°C)	0.107	0.066	0.066
Reflectivity (≥31°C)	0.118	0.066	0.066
Emissivity	0.9	0.9	0.9

To ensure that the simulation process aligns with the actual outdoor exposure environment, this study extracted real-time meteorological data for a specific experimental period from the meteorological database system to serve as environmental boundary conditions. The collected data includes hourly temperature, average wind speed, daily maximum solar radiation, and sunlight duration. These dynamic data were loaded onto the surface of the model in the form of time functions through arrays and looping programs written in APDL. The sides and bottom of the model were set as adiabatic boundaries to simplify the analysis to a one-dimensional vertical heat conduction model.

3. Results and Discussion

3.1 Solar Spectral Reflectance

3.1.1 Spectral Reflectance of Thermochromic Powder

The spectral reflectance of black thermochromic powder at different temperatures is shown in Fig. 4. The reflectance curves of the thermochromic powder exhibit significantly higher solar reflectance, particularly in the infrared range. Below the transition temperature, the reflectance of the thermochromic powder in the visible light range (300nm-700nm) fluctuates around 20%. At the boundary between visible light and near-infrared light, around 780nm, the reflectance value sharply increases and exceeds 80%, then stabilizes. When the temperature exceeds the transition temperature, the reflectance of the thermochromic powder in the visible light range increases significantly, with an increase of over 50%. This is because the higher temperature exceeds the transition temperature, causing the thermochromic powder to lose its color, which in turn increases the reflectance in the visible light range.

Using the previously described method, the solar reflectance of the thermochromic powder in each wavelength band was calculated. As shown in the table 3, the black thermochromic powder

ISSN: 2414-1895 DOI: 10.6919/ICJE.202603_12(3).0014

significantly increases in the ultraviolet, visible, and near-infrared light bands as the temperature rises, with a large Δ RTotal value (23.70%), resulting in a broader temperature regulation range.

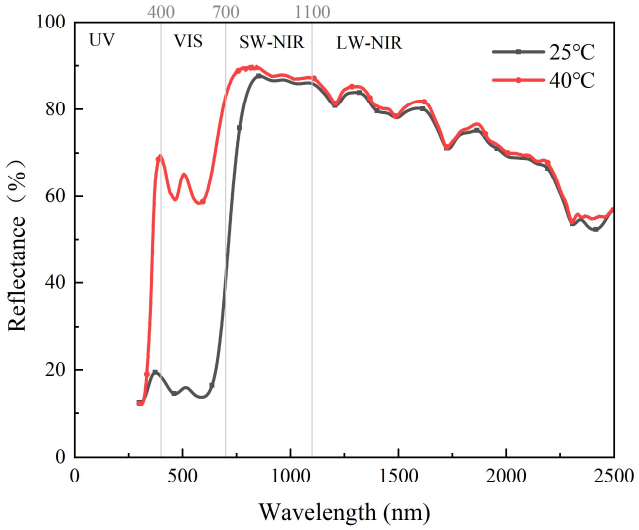

Fig. 4 Black thermochromic powder spectral reflectance

Table 3. Solar reflectance of black thermochromic powder at different wavelength bands.

Solar reflectance (%)	Ruv	Rvis	Rnir	Rtotal
Black thermochromic powder-25°C	17.12	17.03	78.80	49.06
Black thermochromic powder-40°C	41.80	64.16	83.89	72.76

3.1.2 Spectral Reflectance of Thermochromic Asphalt

The spectral reflectance of samples under varying temperature conditions is illustrated in Fig. 5, with the corresponding solar reflectance values for each waveband summarized in Table 4. The results indicate that all samples exhibit a consistent spectral trend: reflectance remains low in the visible light range and rises sharply beyond the 780 nm threshold, marking the transition into the near-infrared spectrum.

At both 25°C and 40°C, increasing the dosage of thermochromic powder significantly shifts the reflectance curves upward. Notably, while the powder dosage has a negligible impact on visible light reflectance below the transition temperature, it triggers a substantial increase at 40°C. Compared to the base light-colored binder, the visible reflectance of the thermochromic asphalt increases with dosage, reaching a maximum enhancement of approximately 73% and a peak total reflectance of 16.4%. This demonstrates that the light-colored binder, due to its low initial chromaticity, effectively amplifies the color-changing effect of the thermochromic material, thereby maximizing its dynamic temperature-regulating potential.

Further comparison reveals distinct mechanisms for reflectance improvement. For the control sample without thermochromic powder, heating primarily increases reflectance in the near-infrared range, while the UV and visible regions remain stable. In contrast, samples containing thermochromic powder show significant reflectance gains across all wavebands at high temperatures. This overall improvement is dual-sourced: the leap in visible reflectance is driven by the lightening of the thermochromic material, whereas the gains in the near-infrared region are predominantly governed by the inherent thermal properties of the light-colored binder.

ISSN: 2414-1895 DOI: 10.6919/ICJE.202603_12(3).0014

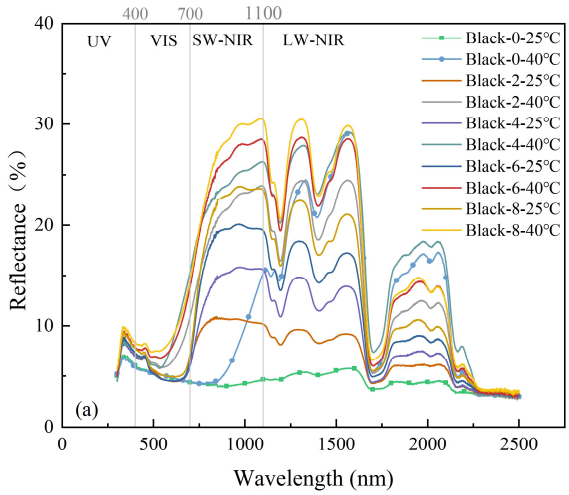

Fig. 5 Solar reflectance of light-colored thermochromic asphalt binders

Data from Table 4 indicate that as the temperature of the control sample (Black-0) increases from 25°C to 40°C, its near-infrared reflectance rises significantly from 4.44% to 11.54%, driving a substantial gain in total solar reflectance. Consequently, the light-colored binder maintains elevated near-infrared reflectance across both temperature states, establishing a robust optical foundation for thermal regulation.

Upon exceeding the transition threshold, the thermochromic binder exhibits a marked surge in visible light reflectance. The alignment between the high-temperature spectral profile and the optical characteristics of the additive confirms that the enhancement in the visible range is primarily driven by the thermochromic powder.

In contrast, traditional 90# asphalt shows no optical response to temperature fluctuations, with its total solar reflectance remaining constant at 3.53%. At 40°C, the Black-6 binder achieves a visible reflectance of 8.16% and a total solar reflectance of 15.46%, representing an 118% increase in visible reflectance and a 4.38-fold improvement in total solar reflectance compared to the conventional asphalt. This comparison underlines the critical role of the light-colored matrix in amplifying the optical modulation effects of thermochromic materials, which are otherwise suppressed in dark-colored binders.

Table 4. Solar reflectance of asphalt binders at different wavelength bands

Solar reflectance (%)	25°C				40°C				
	Ruv	Rvis	Rnir	Rtotal	Ruv	Rvis	Rnir	Rtotal	ΔRtotal (Rtotal at 40 °C − Rtotal at 25 °C)
90#	4.10	3.74	3.27	3.53	4.10	3.74	3.27	3.53	0
Black-0	6.51	5.12	4.44	4.87	6.30	5.09	11.54	8.52	3.65
Black-2	7.70	5.41	8.95	7.41	7.68	6.95	18.45	12.96	5.55
Black-4	7.43	5.32	12.18	9.03	7.58	8.02	21.89	15.18	6.15
Black-6	7.83	5.39	15.34	10.73	8.36	8.16	22.21	15.46	4.73
Black-8	8.32	5.82	17.98	12.30	8.84	8.82	23.45	16.40	4.10

ISSN: 2414-1895 DOI: 10.6919/ICJE.202603_12(3).0014

In summary, the light-colored thermochromic binder developed in this study demonstrates superior reflective performance across both visible and near-infrared ranges compared to traditional 90# asphalt. The light-colored matrix not only provides inherent near-infrared reflectance but also effectively activates the visible-range thermochromic response, resulting in a more efficient and stable temperature-control capability.

3.2 Evaluation of Indoor Temperature Control Effect of Thermochromic Asphalt Mixture

3.2.1 Road Surface Cooling Performance

Fig. 6 illustrate the temperature variation curves of the thermochromic asphalt mixture and the traditional 90# asphalt mixture at different depths as a function of radiation time.

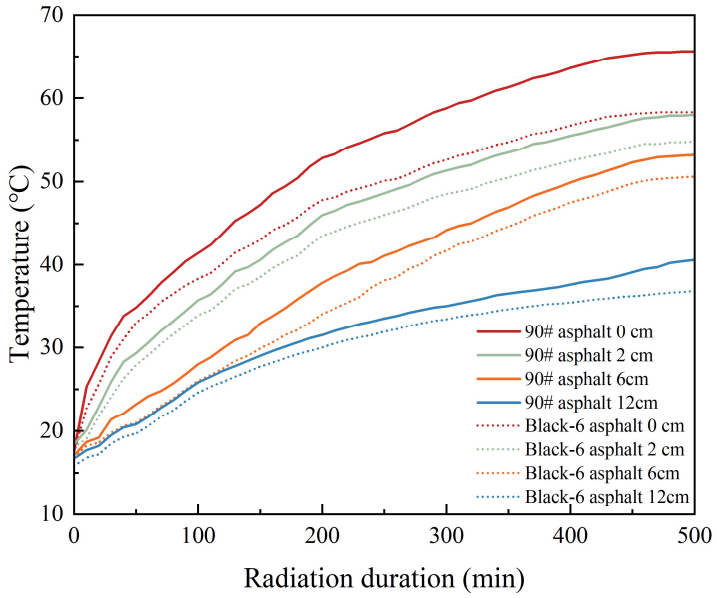

Fig. 6 Temperature evolution of asphalt mixture specimens under indoor temperature-controlled solar irradiation

As illustrated in Fig. 6, the temperature evolution across both asphalt mixture specimens follows a consistent non-linear trajectory throughout the radiation period. This thermal process is characterized by three distinct phases: an initial rapid warming stage during the first 100 minutes where heat absorption dominates; a transitional stage from 100 to 400 minutes where the heating rate decelerates as dissipation strengthens; and a final quasi-steady state after 400 minutes as the system approaches thermal equilibrium. Despite these shared trends, the thermochromic asphalt mixture consistently maintains lower temperatures at all depths compared to the traditional 90# mixture, demonstrating superior thermal resistance.

Pavement surface temperature serves as a primary metric for evaluating road thermal conditions. During the early heating stage from 0 to 60 minutes, the thermochromic specimen exhibits significant thermal inertia, with a surface heating rate lower than the control group and a temperature deficit exceeding 2°C. This confirms that high initial reflectivity effectively suppresses heat input. By the time thermal equilibrium is reached at 500 minutes, the peak surface temperature of the traditional mixture reaches 65.6°C, whereas the thermochromic specimen is limited to 58.3°C. This reduction of 7.3°C indicates that the thermochromic modifier successfully blocks solar radiation at the source by increasing surface reflectivity.

The protective effect of the thermochromic surface layer also extends to the internal temperature field. The cooling impact is most pronounced at a depth of 2 cm, where the temperature profile closely mirrors the surface behavior. At greater depths of 6 cm and 12 cm, despite the inherent lag in heat

ISSN: 2414-1895 DOI: 10.6919/ICJE.202603_12(3).0014

transfer, the thermochromic specimen remains consistently cooler than its traditional counterpart. These results suggest that the thermal shielding effect of the surface layer not only lowers the immediate pavement temperature but also attenuates the downward heat flux, thereby effectively reducing the overall thermal profile of the pavement structure.

3.2.2 Road Surface Thermal Insulation Performance

Pavement temperatures dropping below freezing during winter is a significant factor causing performance degradation. In low-temperature environments, asphalt materials become more brittle and are prone to cracking under thermal contraction stress, which shortens the pavement's service life. Simultaneously, surface icing significantly reduces skid resistance, threatening traffic safety. Therefore, the time required for the pavement to cool to the freezing point is a key indicator for evaluating the winter thermal insulation performance of temperature-control materials. In this test, specimens were placed in a -20°C environmental chamber, and the thermal maintenance capability of the thermochromic materials was assessed by monitoring temperature changes at surface. By performing linear fitting on the cooling data, the time required for each specimen group to drop to 0°C was calculated.

Linear fitting results indicate that the cooling rate of ordinary 90# asphalt is 1.424°C/min, while that of the thermochromic asphalt is only 0.937°C/min. This represents a reduction in cooling speed of approximately 34.2%. The time required for the pavement surface to reach 0°C is a critical safety indicator for winter driving. Ordinary 90# asphalt reaches the freezing point approximately 15.19 minutes after cooling begins, whereas the thermochromic asphalt postpones this until 22.43 minutes. This increase of approximately 47.7% in duration provides a valuable window for anti-icing treatments and effectively reduces the risk of surface icing or thermal contraction cracking caused by sudden, drastic cooling.

This temperature-control performance primarily stems from two factors: first, the thermochromic materials possess higher enthalpy and specific heat capacity, granting the mixture greater thermal inertia; second, when the ambient temperature falls below the transition threshold, the thermochromic powder reverts to a dark state, reducing reflectance and thereby enhancing heat absorption capacity. Traditional heat-reflective cool pavements often cause pavement temperatures to drop far below the ambient temperature in winter due to their constant high reflectance. While maintaining excellent cooling effects in summer, the thermochromic asphalt in this study demonstrates strong thermal inertia and heat retention capabilities in winter. Experiments prove that this material significantly flattens the cooling gradient of the pavement surface in low-temperature environments, allowing the road to maintain a relatively stable thermal state under severe cold conditions and achieving effective dual-season temperature regulation.

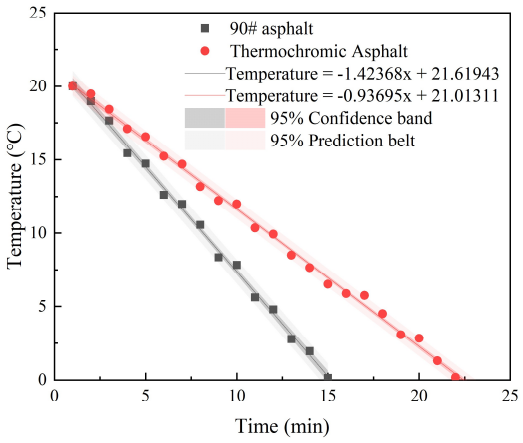

Fig. 7 Asphalt mixture surface temperature at low temperatures

ISSN: 2414-1895 DOI: 10.6919/ICJE.202603_12(3).0014

3.3 Cooling Effect of Thermochromic Asphalt based on Temperature Field Model

3.3.1 Feasibility Verification of Numerical Simulation of Temperature Field

To verify the accuracy of the constructed asphalt pavement temperature field evaluation model, the parameters were validated by comparing the simulated temperature data and measured data for the controlled sample during the outdoor solar radiation test. A temperature sensor was horizontally inserted 2 cm deep into the surface of the Marshall specimen, with the sides and bottom wrapped in thermal insulation cotton, and placed in an open outdoor area to record the internal data in real-time. Meanwhile, meteorological data from the meteorological database system during the outdoor solar radiation test were collected as input parameters for the simulation, as detailed in Table 5. The atmospheric temperature values during the temperature field testing are shown in Table 6.

Table 5. Local meteorological parameter values at the time of actual temperature field measurement

parameter	wind speed (m/s)	Peak solar radiation (W/m^2)	Sunrise time	Sunset time
Value	1.82	327	6:44	18:08

Table 6. Ambient air temperature during temperature field testing

Time (Hour)	Time (Sec)	Ambient temperature (℃)
1:00	3600	24.1
2:00	7200	24.6
3:00	10800	24.5
4:00	14400	24.7
5:00	18000	24.5
6:00	21600	24.6
7:00	25200	25.2
8:00	28800	24.4
9:00	32400	24.1
10:00	36000	25
11:00	39600	27.3
12:00	43200	27.6
13:00	46800	29.1
14:00	50400	30.3
15:00	54000	30.4
16:00	57600	29.6
17:00	61200	30.3
18:00	64800	29.9
19:00	68400	29.1
20:00	72000	28.5
21:00	75600	28.1
22:00	79200	27.8
23:00	82800	27.7
24:00	86400	27.4

ISSN: 2414-1895 DOI: 10.6919/ICJE.202603_12(3).0014

Finally, the actual measurement results were compared with the road surface temperatures obtained from the numerical simulation of the constructed temperature field model, and the results are shown in Fig 8.

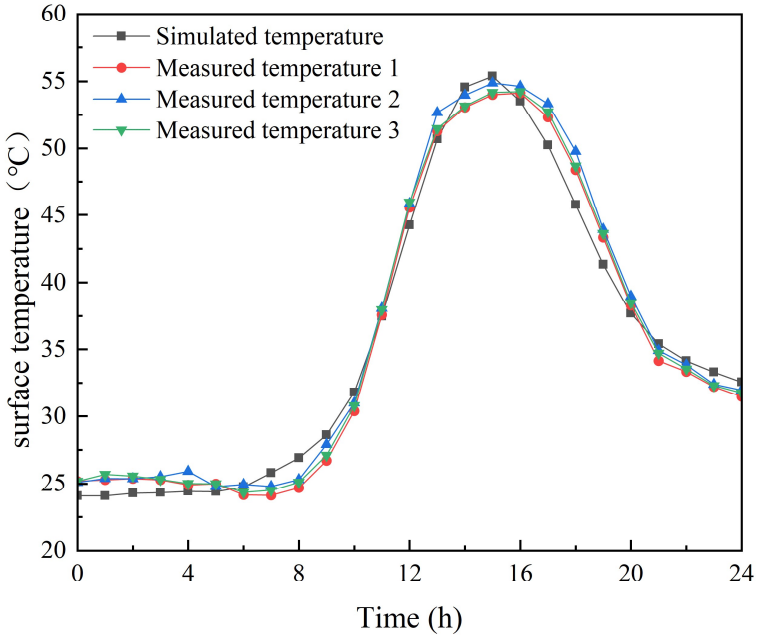

Fig. 8 Comparison of numerical simulation surface temperature and measured temperature

Upon comparison, the simulated temperature variation path aligns closely with the measured values, with the two curves largely overlapping. To quantitatively evaluate the consistency between the model and the experiment, the Mean Relative Error (MRE) between the theoretical simulated values and the corresponding measured values was calculated over the 0–24 hour period. The maximum error recorded was 3.89%, which is below the 5% threshold. This effectively demonstrates that the constructed model can accurately reproduce the actual thermal process and possesses high precision.

$$\mathrm{MRE} = \frac{1}{25}\sum_{i=0}^{24}\left|\frac{T_{m,i} - T_{s,i}}{T_{m,i}}\right| \times 100\% \tag{11}$$

Where i represents time (h); $T_{m,i}$ represents the measured temperature data at time i (°C); and $T_{s,i}$ represents the simulated temperature data at time i (°C).

3.3.2 Evaluation of Cooling Effects Across Different Regions

After verifying the reliability of the model, this study combined local meteorological parameters with numerical simulation to compare and analyze the temperature performance of thermochromic asphalt versus ordinary base asphalt pavement surfaces across different climatic regions. This comparison aims to evaluate the practical cooling efficiency of thermochromic asphalt over a broader geographical range. According to the national standard *Design Code for General Principles of Civil Buildings* (GB50352-2005), China is divided into seven main climatic zones. To this end, we screened meteorological data from the China Meteorological Database for typical cities representing these zones for July and August of the summer of 2025 for temperature field simulation. The climatic

ISSN: 2414-1895 DOI: 10.6919/ICJE.202603_12(3).0014

characteristics and reasons for selecting these typical cities are listed in the table below, and the relevant data were further processed as boundary input conditions for the pavement temperature field simulation.

Table 7. Typical urban climate characteristics used for temperature field simulation

Climate Zone	Climatic Characteristics	City
Zone I: Severe Cold Region	Severe and long winters; short, cool and pleasant summers.	Harbin
Zone II: Cold Region	Cold and dry winters; hot and humid summers.	Beijing
Zone III: Hot Summer & Cold Winter Region	Hot and sultry summers (hottest month mean temperature 25-30°C, humidity approx. 80%).	Wuhan
Zone III: Hot Summer & Cold Winter Region	Hot and sultry summers; high humidity.	Shanghai
Zone IV: Hot Summer & Warm Winter Region	Long summers and no winters; hot and long-duration summers with high humidity.	Guangzhou
Zone V: Temperate Region	Mild all year round; cool and pleasant summers.	Kunming
Zone VI: Severe Cold Region (High Plateau)	Severe winters; cool summers (July mean temperature < 18°C).	Lhasa
Zone VII: Severe Cold Region (Arid)	Severe winters; hot and dry summers (July mean temperature > 18°C, humidity < 50%).	Urumqi
Supplement: Temperate Continental Climate	Cold winters and hot summers; large annual and diurnal temperature ranges; scarce precipitation.	Lanzhou
Supplement: Tropical Monsoon Climate	High temperatures year-round; rainy summers.	Haikou

The meteorological data, including average wind speed, daily average air temperature, and short-wave radiation for the ten cities under typical summer high-temperature conditions, were incorporated into the simulation as environmental loads. Consequently, the time-varying curves for road surface temperatures were obtained for both the thermochromic asphalt and the control group (base asphalt pavement) across these ten cities.

As shown in Figs 9 and 10, the overall trend indicates that the daytime temperature curves for thermochromic asphalt pavements are significantly lower than those of traditional asphalt pavements across all ten city conditions. Regarding the specific magnitude of temperature reduction, the cooling effect of thermochromic asphalt exhibits significant regional variation. In cities with intense solar radiation, the peak temperature of the thermochromic asphalt pavement is markedly lower than that of the traditional pavement, reflecting its superior cooling performance under high-radiation conditions. Furthermore, the cooling effect of thermochromic asphalt is not constant throughout the day; the temperatures of both pavements are relatively close during the early morning and evening. However, the divergence between the two curves is most pronounced around noon when solar radiation reaches its peak. This confirms the dynamic temperature-regulation characteristics of thermochromic materials, which enhance reflection only during high-temperature periods when cooling is required, while not affecting the pavement's heat absorption during low-temperature periods. This behavior helps mitigate thermal stress caused by diurnal temperature fluctuations.

ISSN: 2414-1895 DOI: 10.6919/ICJE.202603_12(3).0014

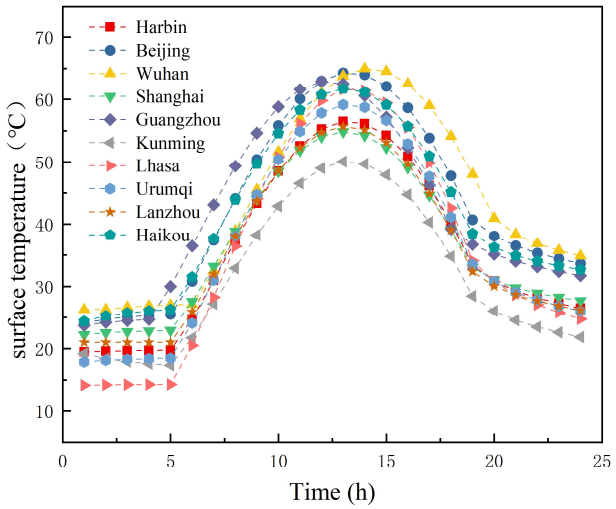

Fig. 9 Surface temperatures of traditional asphalt pavements under different urban conditions

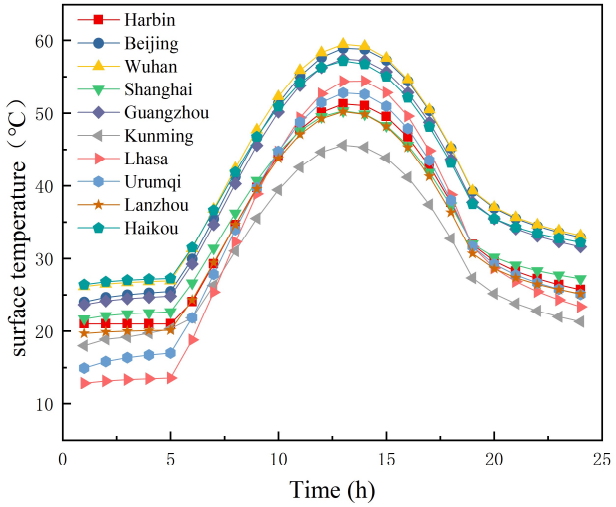

Fig. 10 Surface temperatures of thermochromic asphalt pavements under different urban conditions

Table 8 summarizes the selected meteorological conditions for different cities and the maximum road surface temperatures of base asphalt pavement and thermochromic asphalt pavement obtained through numerical simulation. As shown in the table, the simulated application of thermochromic asphalt across ten different climatic regions achieved an effective cooling range of 4.443°C to 7.260°C.

Comparative analysis of the meteorological conditions in different cities reveals that the cooling performance of thermochromic asphalt is primarily influenced by solar radiation intensity. The higher the short-wave solar radiation value of a city, the more pronounced the cooling effect becomes. For instance, in Lhasa, the peak summer daily radiation reaches as high as 1100 W/m², the highest among the ten cities. Under these strong radiation conditions, the thermochromic asphalt fully leverages its optical response characteristics, achieving a maximum temperature reduction of 7.26°C compared to base asphalt.

In addition to radiation, ambient air temperature and wind speed exert a synergistic influence on the cooling effect. In cities with similar radiation intensities, a higher ambient temperature typically

ISSN: 2414-1895 DOI: 10.6919/ICJE.202603_12(3).0014

implies a larger baseline for cooling potential; for example, Guangzhou and Beijing exhibit similar performance. Conversely, although Shanghai has higher radiation values, its average wind speed of 3.41 m/s is the highest in the sample. Stronger convective heat transfer accelerates the dissipation of heat from the pavement, resulting in a lower baseline temperature for the base asphalt pavement, which leads to a relatively smaller cooling margin for the thermochromic asphalt. The simulation results confirm that thermochromic asphalt holds significant application value in addressing pavement overheating in regions with high temperatures and strong radiation. Its potential for improving thermal comfort is particularly prominent in plateau and inland cities with abundant solar radiation resources.

Table 8. Meteorological conditions and cooling effects of thermochromic asphalt pavement materials in different regionsn

City	Average wind speed(m/s)	average temperature(℃)	Peak solar radiation(W/m^2)	Maximum temperature of base asphalt(℃)	Maximum temperature of thermochromic asphalt(℃)	Temperature drop(℃)
Harbin	1.88	24.9	970	56.476	51.247	5.229
Beijing	1.71	32.0	1000	64.306	58.929	5.377
Wuhan	2.10	33.0	1040	64.978	59.458	5.520
Shanghai	3.41	28.5	1020	54.836	50.289	4.547
Guangzhou	1.90	31.0	1010	62.891	57.446	5.445
Kunming	1.82	20.4	880	50.039	45.596	4.443
Lhasa	1.05	19.49	1100	61.628	54.368	7.260
Urumqi	2.02	24.1	1090	59.157	52.775	6.382
Lanzhou	2.80	26.0	1040	55.683	50.189	5.494
Haikou	3.10	33.0	1080	61.736	57.165	4.571

4. Conclusion

In this study, a novel thermochromic asphalt pavement was developed and its temperature control performance was evaluated through experimental and numerical methods. The main conclusions are as follows:

(1) The developed light-colored binder provides a robust optical foundation for the pavement. It offers inherent near-infrared reflectance and successfully amplifies the visible-range color-changing response of the thermochromic powder. This combination effectively resolves the optical masking issue commonly found in traditional dark asphalt.

(2) The thermochromic binder exhibits high sensitivity to temperature changes. Above the threshold of 31℃, the total solar reflectance of the material increases significantly and outperforms traditional 90# asphalt. This increase is driven by a dual mechanism where the thermochromic powder regulates visible light while the light-colored binder enhances near-infrared reflection.

(3) Indoor tests confirm excellent summer cooling and winter insulation capabilities. In simulated summer conditions, the material achieves a peak surface temperature reduction of 7.3℃. In simulated winter conditions, it slows the cooling process by 34.2% and extends the time required to reach the freezing point from 15.19 to 22.43 minutes. This delay is crucial for preventing icing and thermal cracking.

(4) Finite element method simulations show that cooling efficiency is primarily governed by solar radiation intensity. The material demonstrates high application value across various climates in China with cooling margins ranging from 4.44 to 7.26℃. It is particularly effective in high-altitude and inland regions with intense radiation such as Lhasa and Wuhan.

ISSN: 2414-1895 DOI: 10.6919/ICJE.202603_12(3).0014

In summary, this thermochromic asphalt offers a smart approach to pavement thermal management. It contributes to improved road durability and driving safety while mitigating the urban heat island effect.

References

[1] H. Li, A. Saboori, X. Cao, Information synthesis and preliminary case study for life cycle assessment of reflective coatings for cool pavements, International Journal of Transportation Science and Technology 5 (2016) 38–46. https://doi.org/10.1016/j.ijtst.2016.06.005.

[2] R.S. Benrazavi, K. Binti Dola, N. Ujang, N. Sadat Benrazavi, Effect of pavement materials on surface temperatures in tropical environment, Sustainable Cities Soc. 22 (2016) 94–103. https://doi.org/10.1016/j.scs.2016.01.011.

[3] B. Arregi, I. Lopez-Villamor, D. Zamora-Sanchez, R. Garay-Martinez, Impact of Pavement Material Properties on Radiant Heat Exchanges with the Built Environment, in: 2025 10th International Conference on Smart and Sustainable Technologies (SpliTech), IEEE, Bol and Split, Croatia, 2025: pp. 1–5. https://doi.org/10.23919/SpliTech65624.2025.11091742.

[4] A. Mohajerani, J. Bakaric, T. Jeffrey-Bailey, The urban heat island effect, its causes, and mitigation, with reference to the thermal properties of asphalt concrete, J. Environ. Manage. 197 (2017) 522–538. https://doi.org/10.1016/j.jenvman.2017.03.095.

[5] Y. Wardeh, E. Kinab, G. Escadeillas, P. Rahme, S. Ginestet, Review of the optimization techniques for cool pavements solutions to mitigate Urban Heat Islands, Build. Environ. 223 (2022) 109482. https://doi.org/10.1016/j.buildenv.2022.109482.

[6] M. Guo, R. Zhang, X. Du, P. Liu, A State-of-the-Art Review on the Functionality of Ultra-Thin Overlays Towards a Future Low Carbon Road Maintenance, Engineering 32 (2024) 82–98. https://doi.org/10.1016/j.eng.2023.03.020.

[7] Y. Wardeh, P. Rahme, G. Escadeillas, E. Kinab, S. Ginestet, Thermophysical experimental characterisation of concrete cool pavements, Int. J. Pavement Eng. 25 (2024) 2438851. https://doi.org/10.1080/10298436.2024.2438851.

[8] M. Guo, M. Zhou, X. Du, P. Liu, Machine learning-based analysis of interaction effects among influencing factors on the resilient modulus of stabilized aggregate base, Computer Aided Civil Eng 40 (2025) 5253–5268. https://doi.org/10.1111/mice.70102.

[9] B.R. Anupam, U.C. Sahoo, A.K. Chandrappa, P. Rath, Emerging technologies in cool pavements: A review, Constr. Build. Mater. 299 (2021) 123892. https://doi.org/10.1016/j.conbuildmat.2021.123892.

[10] J. Wang, J. Zhao, X. Xu, M. Zhang, Y. Liu, R. Bai, Y. Wang, X. Kong, Study on the Solar-Thermal Effect Mechanism and Energy Balance Relationship of Heat-Reflective Pavement Model in Cold Region, (2024). https://doi.org/10.2139/ssrn.5049419.

[11] P.H.N. Crosby, A.N. Netravali, Green Thermochromic Materials: A Brief Review, Adv. Sustainable Syst. 6 (2022) 2200208. https://doi.org/10.1002/adsu.202200208.

[12] L. Civan, S. Kurama, A review: Preparation of functionalised materials/smart fabrics that exhibit thermochromic behaviour, Mater. Sci. Technol. 37 (2021) 1405–1420. https://doi.org/10.1080/02670836.2021.2015844.

[13] J. Hu, X. (Bill) Yu, Innovative thermochromic asphalt coating: characterisation and thermal performance, Road Materials and Pavement Design 17 (2016) 187–202. https://doi.org/10.1080/14680629.2015.1068215.

[14] J. Hu, X. (Bill) Yu, Experimental Study of Sustainable Asphalt Binder: Influence of Thermochromic Materials, Transp. Res. Rec.: J. Transp. Res. Board 2372 (2013) 108–115. https://doi.org/10.3141/2372-12.

[15] J. Hu, N. Wanasekara, X. (Bill) Yu, Thermal properties of thermochromic asphalt binders by modulated differential scanning calorimetry, Transportation Research Record: Journal of the Transportation Research Board 2444 (2014) 142–150. https://doi.org/10.3141/2444-16.

[16] Z. You, M. Zhang, R. Bai, A review of the near-infrared reflective coatings for cooling asphalt pavements in permafrost regions, Constr. Build. Mater. 498 (2025) 143898. https://doi.org/10.1016/j.conbuildmat.2025.143898.

ISSN: 2414-1895 DOI: 10.6919/ICJE.202603_12(3).0014

[17] T. Karlessi, M. Santamouris, K. Apostolakis, A. Synnefa, I. Livada, Development and testing of thermochromic coatings for buildings and urban structures, Sol. Energy 83 (2009) 538–551. https://doi.org/10.1016/j.solener.2008.10.005.

[18] P. Tang, L. Mo, C. Pan, H. Fang, B. Javilla, M. Riara, Investigation of rheological properties of light colored synthetic asphalt binders containing different polymer modifiers, Constr. Build. Mater. 161 (2018) 175–185. https://doi.org/10.1016/j.conbuildmat.2017.11.098.

[19] H.C. Zhang, J. Wu, Y. Luo, Z. Qin, High-temperature properties of composite modified light-colored synthetic asphalt binders, Mater. Res. Express 8 (2021) 065305. https://doi.org/10.1088/2053-1591/ac07e6.

[20] X. Pei, W. Fan, S. Chen, Investigation on the performance of colored asphalt and pavement, IOP Conf. Ser.: Earth Environ. Sci. 514 (2020) 052016. https://doi.org/10.1088/1755-1315/514/5/052016.

[21] X. Zhang, H. Li, M. Jia, N. Xie, I. Kousis, M. Santamouris, Laboratorial investigation on optical, thermal and pavement performance of biomimetic dark reflective coatings with composite structure for pavement cooling, Build. Environ. 266 (2024) 112057. https://doi.org/10.1016/j.buildenv.2024.112057.

[22] M. Santamouris, Using cool pavements as a mitigation strategy to fight urban heat island-A review of the actual developments, Renewable Sustainable Energy Rev. 26 (2013) 224–240. https://doi.org/10.1016/j.rser.2013.05.047.